Field-driven collapsing dynamics of skyrmions in magnetic multilayers

R. Tomasello [1,*,†] Z. Wang [2,3,*] E. Raimondo [4] S. Je [5] M. Im,[5] M. Carpentieri [1] W. Jiang,[2,3,‡] and G. Finocchio [4,§]

[1]*Department of Electrical and Information Engineering, Politecnico di Bari, Bari 70125, Italy*
[2]*State Key Laboratory of Low-Dimensional Quantum Physics and Department of Physics, Tsinghua University, Beijing 100084, China*
[3]*Frontier Science Center for Quantum Information, Tsinghua University, Beijing 100084, China*
[4]*Department of Mathematical and Computer Sciences, Physical Sciences and Earth Sciences, University of Messina, I-98166 Messina, Italy*
[5]*Center for X-ray Optics, Lawrence Berkeley National Laboratory, Berkeley, California 94720, USA*

Magnetic skyrmions are fascinating topological particle-like textures which are promoted by a trade-off among interfacial properties (perpendicular anisotropy and Dzyaloshinskii-Moriya interaction) and dipolar interactions. Depending on the dominant interaction, complex spin textures, including pure Néel and hybrid skyrmions, have been observed in magnetic multilayers. A quantification of these different spin textures typically requires a depth-reoslved magnetic imaging or scattering techniques. In the present work, we will show qualitatively different collapsing dynamics for pure Néel and hybrid skyrmions induced by a perpendicular magnetic field in two representative systems, $[Pt/Co/Ir]_{15}$ and $[Ta/CoFeB/MgO]_{15}$ multilayers. Skyrmions in the former stack undergo a first morphological transition at zero field to labyrinth domains, and followed by a second morphological transition to skyrmions with opposite chirality and polarity, upon reversing the direction of perpendicular fields. On the other hand, skyrmions in $[Ta/CoFeB/MgO]_{15}$ multilayers exhibit a continuous transition as a function of the field, which is mainly linked to a reversible change of the skyrmion size. A full micromagnetic phase diagram is presented to identify these two collapsing mechanisms as a function of material parameters. Since the two distinct collapsing dynamics rely on the detailed layer-dependent spin structures of skyrmions, we propose to use them as potential fingerprints for identifying the type of skyrmions in magnetic multilayers. Our work could be important for employing pure and hybrid skyrmions for specific applications, due to the strong correlation between the skyrmion dynamics and three-dimensional spin profiles.

I. INTRODUCTION

Magnetic skyrmions have been receiving growing attentions in the last decades. Since the first theoretical predictions on the fundamental and promising properties of these "topologically protected" solitons [1–4], great efforts have driven the development of materials for the experimental stabilization of skyrmions. The first experimental observations regarded B_{20} compounds, where the bulk Dzyaloshinskii-Moriya interaction (DMI) promotes the formation of Bloch skyrmions [5–10]. Later on, increasing interests have been devoted to thin films and heterostructures where ferromagnetic layers (FM) are coupled with materials having strong spin-orbit coupling including heavy metals (HM) [11]. These latter systems allow for the stabilization of skyrmions at room temperature and above, which is a fundamental requirement for practical applications [12]. For example, skyrmions were observed in a variety of thin-film materials, including HM/single-layer FM/oxide [13–15], $HM_1/FM/HM_2$ multilayers [16–24], HM/ferrimagnet/oxide multilayers [25,26],

synthetic antiferromagnets [27–29], as well as hybrid systems [30,31]. The use of $HM_1/FM/HM_2$ multilayers, with the right choice of HM_1 and HM_2, for stabilizing skyrmion is favorable over other solutions for two reasons [16]: (i) the use of asymmetric interfaces, by combining HMs having an opposite sign of interfacial DMI, enhances the effective DMI, thus allowing the stabilization of sub-100-nm skyrmion; and (ii) the skyrmion magnetic volume increases since the skyrmion extends along the thickness direction through the whole multilayer, as a result of the magnetostatic coupling. This allows the skyrmion to be less sensitive to the thermal fluctuations. The static skyrmion profile and chirality in $HM_1/FM/HM_2$ multilayers result from the competition between magnetostatic and interfacial DMI fields [23,32]. At zero or low interfacial DMI (IDMI) values, the magnetostatic field is dominant and skyrmions exhibit a thickness-dependent spin chirality along the thickness direction of the multilayer, which are known as hybrid skyrmions. When the IDMI is high, homogenous Néel skyrmions throughout the thickness——known as pure Néel skyrmions [32,33]——can be achieved.

The different chirality of skyrmions can strongly influence their current-driven dynamics [32,34]. Therefore, understandings of the three-dimensional profile of skyrmions in different materials systems are crucial for spintronic applications. The thickness-dependent chirality can be directly observed in domain walls via the circular dichroism x-ray resonant magnetic

*These authors contributed equally to this work.
†riccardo.tomasello@poliba.it
‡jiang_lab@tsinghua.edu.cn
§gfinocchio@unime.it

scattering [23,32]; those results are then used to identify the type of skyrmions, i.e., hybrid or pure Néel. Recently, an indirect procedure based on the first-order reversal-curve (FORC) technique has been proposed, which suggests systems with pure Néel skyrmion and hybrid skyrmion exhibit different characteristics in the FORC diagrams [33].

Here, we propose a strategy to identify the type of skyrmions stabilized in a magnetic multilayer, i.e., pure Néel or hybrid skyrmions, by performing imaging of the evolution of the spin textures as a function of out-of-plane magnetic fields. Two typical multilayers were characterized experimentally: [Pt/Co/Ir]$_{15}$ with a stronger IDMI and [Ta/CoFeB/MgO]$_{15}$ with a lower IDMI, respectively. The former shows a morphological transition from the skyrmion state to the labyrinth domains. By contrast, a reversible skyrmion state that expands or shrinks according to the field is observed in the latter system. We further perform micromagnetic simulations to explore the thickness-dependent chirality of skyrmions, which confirm the presence of two different types of skyrmions. A detailed understanding of the collapsing dynamics is obtained through calculating the complete phase diagram that summarizes the dynamics on material-specific parameters. Our results can be used as a procedure for characterizing the spin profile of skyrmions in multilayers, which could be useful for future skyrmionic applications, since the dynamics of skyrmions, such as the skyrmion Hall angle, are deeply affected by their static three-dimensional profiles.

II. EXPERIMENTAL MEASUREMENTS

A. Experimental results: Sample description and characterization

Samples No. 1 [Pt(1.5 nm)/Co(1 nm)/Ir(1.5 nm)]$_{15}$ and No. 2 [Ta(3 nm)/Co$_{20}$Fe$_{60}$B$_{20}$(1 nm)/MgO(2 nm)]$_{15}$ multilayers (values in parentheses present the thickness) were deposited onto thermally oxidized silicon substrates using an ultrahigh-vacuum magnetron sputtering system, as schematics illustrated in Figs. 1(a) and 1(c), respectively. Both multilayers are known for hosting the nanoscale skyrmions at room temperature [12,16,17] as a result of IDMI. The magnetic properties of these samples were characterized via using a superconductor quantum interference device magnetometer (MPMS, Quantum Design), results of which are shown in Figs. 1(b) and 1(d) for the multilayers [Pt/Co/Ir]$_{15}$ and [Ta/Co$_{20}$Fe$_{60}$B$_{20}$/MgO]$_{15}$, respectively. There, one can find the corresponding in-plane and out-of-plane magnetic hysteresis loops, which are consistent with typical skyrmion-hosting multilayers. The saturation magnetization and anisotropy field are estimated to be $M_s = $ 1200 emu/cc and $\mu_0 H_k = 500$ mT for the [Pt/Co/Ir]$_{15}$ multilayer, and $M_s = 900$ emu/cc and $\mu_0 H_k = 1000$ mT for the [Ta/Co$_{20}$Fe$_{60}$B$_{20}$/MgO]$_{15}$ multilayer, respectively. These multilayers were also deposited on the 100-nm-thick Si$_3$N$_4$ membranes (Clean SiN, Suzhou) for imaging characterization by using the full-field soft x-ray transmission microscopy with a spatial resolution approaching 20 nm, which is performed at the beamline 6.1.2, Advanced Light Source, Lawrence Berkeley National Laboratory. This imaging approach allows us
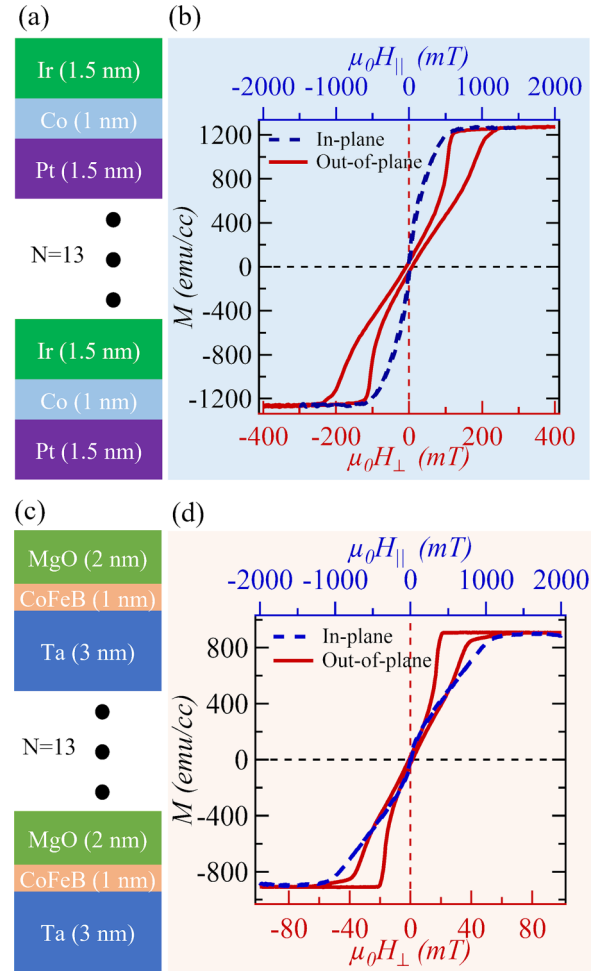

FIG. 1. (a) Schematic illustration of the [Pt(1.5 nm)/Co(1 nm)/Ir(1.5 nm)]$_{15}$ multilayer. (b) Obtained in-plane and out-of-plane magnetic hysteresis loops. (c) Schematic illustration of the [Ta(3 nm)/Co$_{20}$Fe$_{60}$B$_{20}$(1 nm)/MgO(1.5 nm)]$_{15}$ multilayer. (d) Corresponding in-plane and out-of-plane magnetic hysteresis loops. $H_\perp$ and $H_\parallel$ represents the applied magnetic fields that are parallel and perpendicular to the film plane, respectively.

to capture the collapsing dynamics of Néel- or hybrid-type skyrmions that are driven by out-of-plane magnetic fields.

B. Experimental results: Hysteresis measurements

A series of the [Pt/Co/Ir]$_{15}$ magnetic images collected at the Co L$_3$ edge (778.5 eV) under perpendicular fields $H_\perp$ is given in Fig. 2(a). At $\mu_0 H_\perp = 141$ mT, we observe the presence of isolated quasicircular Néel skyrmions. As magnetic fields decrease to zero, these Néel skyrmions are expanded and deformed in shape, i.e., a mixed phase of isolated larger skyrmions and elongated ones is obtained. Upon inverting the direction of magnetic field, this phase is converted into a labyrinthine domain configuration (at $\mu_0 H_\perp = -92.3$ mT). A further increase of magnetic field dissects labyrinthine domains into isolated skyrmions with a reversed magnetization of the core of skyrmion.

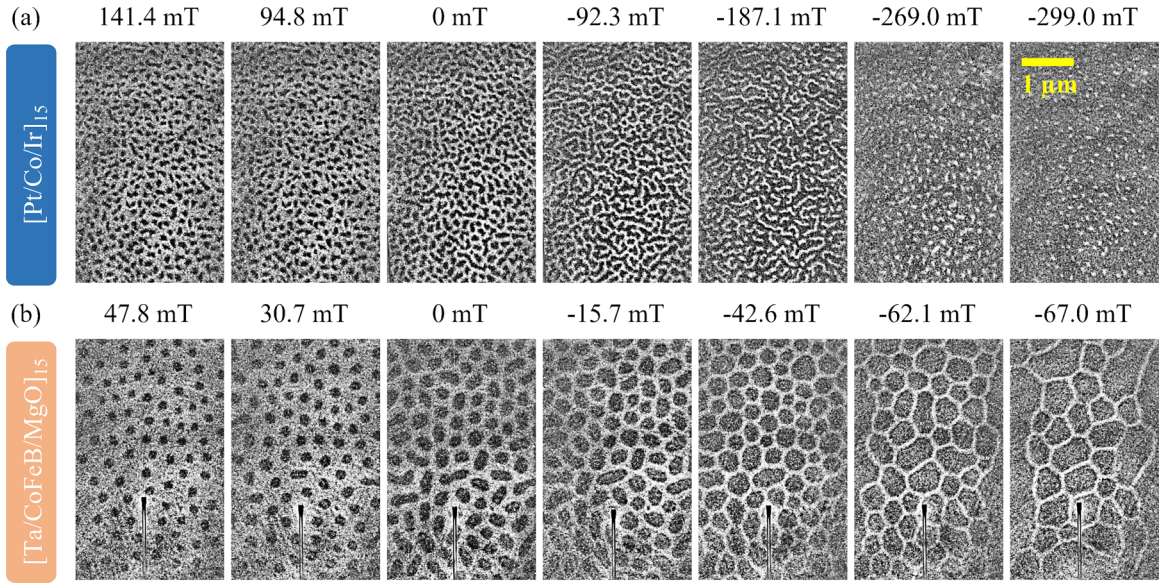By contrast, a very different collapsing phenomenon has been found in the [Ta/CoFeB/MgO]$_{15}$ multilayer. Its

FIG. 2. Experimental observations of the field-driven collapsing dynamics of skyrmions in (a) $[Pt/Co/Ir]_{15}$ and (b) $[Ta/CoFeB/MgO]_{15}$ multilayers. Note that the white color corresponds to the local magnetization pointing out of the film ($m > 0$) and vice versa.

magnetic images were conducted at the Fe $L3$ edge (708.5 eV) under varied $H_\perp$, as shown in Fig. 2(b). The existence of circular domains at $H_\perp = 47.8$ mT is assumed to be the isolated hybrid skyrmions. Initially, the size of these skyrmions increases with a decreased $H_\perp$ magnitude until 0 mT. As the direction of field is reversed, which then becomes parallel to the skyrmion core direction, the hybrid skyrmions continuously expand. A further increase of $H_\perp$ results in the skyrmions to coalesce and form large band domains, with the core magnetization orienting along the field direction (at $\mu_0 H_\perp = -67.0$ mT).

It is clear that the field-driven collapsing dynamics are dramatically different in the $[Pt/Co/Ir]_{15}$ and $[Ta/CoFeB/MgO]_{15}$ multilayers. In particular, the experimental results suggest skyrmions in the former multilayer which go through two phase transitions: (1) from isolated skyrmions to labyrinth domains, and (2) from labyrinth domains to skyrmions with opposite core to the initial ones. In the latter material system, a reversible process from isolated skyrmions to large domains is observed, in which the magnetization orientation is along the direction of the core of the original skyrmions. These results imply their different spin profiles across the thickness direction that will be studied by performing micromagnetic simulations.

III. MICROMAGNETIC MODEL

Below, we perform micromagnetic simulations and use an analytical theory to reveal the role of the layered-dependent spin chirality in assisting collapsing dynamics of skyrmions in these two material systems. Micromagnetic computations were performed by means of a state-of-the-art micromagnetic solver, PETASPIN, which numerically integrates the Landau-Lifshitz-Gilbert equation by applying the Adams-Bashforth time-solver scheme [35]:

$$\frac{d\mathbf{m}}{d\tau} = -(\mathbf{m} \times \mathbf{h}_{\text{eff}}) + \alpha_G \left(\mathbf{m} \times \frac{d\mathbf{m}}{d\tau} \right), \quad (1)$$

where $\mathbf{m} = \mathbf{M}/M_s$ is the normalized magnetization vector, α_G is the Gilbert damping, and $\tau = \gamma_0 M_s t$ is the dimensionless time, with γ_0 being the gyromagnetic ratio and M_s the saturation magnetization. $\mathbf{h}_{\text{eff}}$ is the normalized effective magnetic field, which includes the exchange, IDMI, uniaxial anisotropy, and external perpendicular magnetic fields, as well as the magnetostatic field computed by calculating the magnetostatic energy of the whole system.

We study two set of samples that were signified by very different material specific parameters, No. 1 and No. 2, characterized by five repetitions of ferromagnet layer of thickness 1 nm. For sample No. 1 hosting a pure Néel skyrmion, we used typical parameters values of $[Pt/Co/Ir]_{15}$ multilayers [16]: saturation magnetization $M_s = 1.2$ MA/m, $K_u = 1.29$ MJ/m^3, exchange constant $A = 10$ pJ/m, IDMI parameter $D = 2.5$ mJ/m^2, and a discretization cell size of $2.5 \times 2.5 \times 1$ nm^3, and $400 \times 400 \times 17$ computational cells, whereas for sample No. 2 hosting a hybrid skyrmion, we used typical parameters values of $[Ta/CoFeB/MgO]_{15}$ multilayers [23]: $M_s = 0.91$ MA/m, $K_u = 0.52$ MJ/m^3, exchange constant $A = 10$ pJ/m, IDMI parameter $D = 0.5$ mJ/m^2, and a discretization cell size of $4 \times 4 \times 1$ nm^3, and $250 \times 250 \times 21$ computational cells. The ferromagnetic layers are coupled to one another by means of only the magnetostatic field (exchange-decoupled layers), and are separated by a 3- and 4-nm-thick nonmagnetic layer for samples No. 1 and No. 2, respectively. All the simulations were performed with IDMI boundary conditions $\frac{d\mathbf{m}}{dn} = \frac{D}{2A}(\hat{z} \times \mathbf{n}) \times \mathbf{m}$ [36,37], where $\mathbf{n}$ is the unit vector normal to the sample edge.

IV. RESULTS AND DISCUSSION

A. Micromagnetic results: Comparison of pure Néel and hybrid skyrmions

Figure 3 shows the two equilibrium configurations of skyrmions in these two multilayers. For sample No. 1, a Néel skyrmion is observed in all the layers, suggesting the
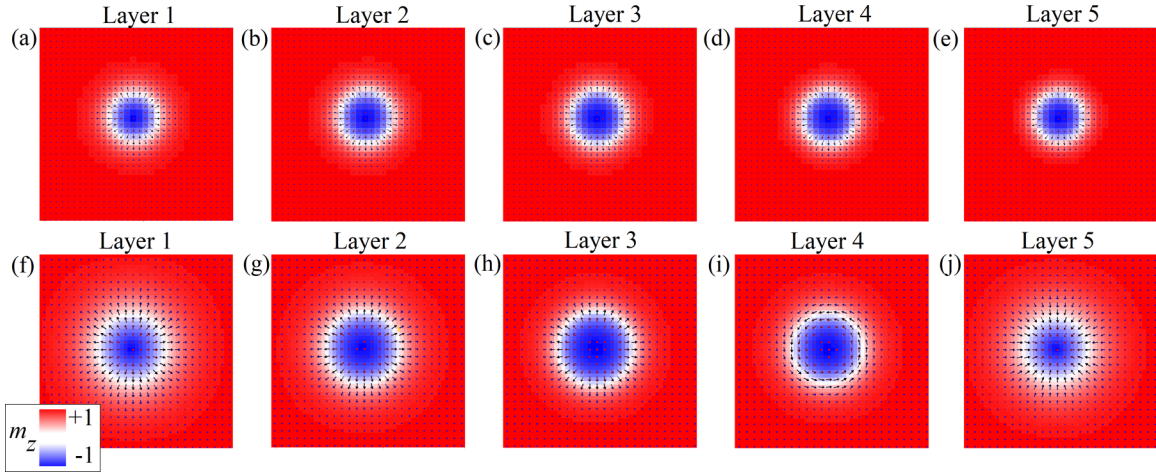
FIG. 3. Equilibrium configurations of skyrmions as obtained by micromagnetic simulations in the *x-y* plane. (a)–(e) Néel skyrmions in the five-repetition [Pt/Co/Ir]$_{15}$ multilayer for $\mu_0 H_\perp = 141$ mT. (e)–(h) Hybrid skyrmions in the five-repetition [Ta/CoFeB/MgO]$_{15}$ multilayer for $\mu_0 H_\perp = 47.9$ mT.

independence of chirality on thickness due to the large contribution from IDMI. In sample No. 1, the effect of the magnetostatic field can only be observed in the depth-dependent size of the skyrmion, which is smaller in the external layers and bigger in the middle layer. On the other hand, for sample No. 2 with a smaller IDMI, a hybrid skyrmion is stabilized, where the skyrmion undergoes the transformation along the multilayer thickness from Néel with outward chirality in the bottom layer (layer 1), to Bloch with counterclockwise chirality in layer 4, and to Néel with inward chirality in the top layer (layer 5) [32]. The Bloch skyrmion is not located in the middle layer because of the finite $D = 0.5$ mJ/m^2 [23,32,33]. Our micromagnetic simulations results confirm the above assumption of the existence of two different types of skyrmions in these two distinct multilayers.

B. Micromagnetic results: Field scan as a function of the out-of-plane field

We start the simulations with an initial state containing six pure Néel skyrmions in sample No. 1 at perpendicular external field $\mu_0 H_\perp = 141$ mT, and nine hybrid skyrmions in sample No. 2 at $\mu_0 H_\perp = 47.8$ mT (see Fig. 4). The purpose is to try to reproduce the experimental dynamics in Fig. 2. We gradually reduce the applied field and trace the evolution of the skyrmions. In sample No. 1, at $\mu_0 H_\perp = 141$ mT, skyrmions are small, isolated, and circularly shaped, which is in agreement with our experimental results and with the ones in high-DMI multilayers [33]. As the field decreases to zero, skyrmions become larger, elongated, and deformed in shape. When the field is reversed, such a phase is converted into a labyrinth-domain configuration (see $\mu_0 H_\perp = -92.3$ mT). A further increase of field breaks the labyrinth domain into small skyrmions with a reversed core.

In sample No. 2, the isolated hybrid skyrmions at $\mu_0 H_\perp = 47.9$ mT increase in size and deform into an elongated worm-like shape as the field is reduced to zero. When the field is reversed, which then becomes parallel to the skyrmion core direction, the hybrid skyrmions keep expanding until they start to coalesce and form large band domains, with the

magnetization orienting along the same direction of the applied field ($\mu_0 H_\perp = -29.8$ mT). All the previous numerical results are in agreement with the experimental observations in Fig. 2.

C. Micromagnetic results: Explanation

The origin of the two different collapsing dynamics will be studied. In sample No. 1, a skyrmion with a Néel chirality in all the layers is stabilized by a large IDMI; therefore, its energetic stability can be described by using the same argument as a Néel skyrmion in a single ferromagnetic layer [38]. Figure 5 shows the evolution of energy as a function of the applied field of a single-layer Néel skyrmion and uniform states. This is done by minimizing the energy functional, $E[\mathbf{m}] = \int dV \varepsilon(\mathbf{m})$, with the energy density [38]

$$\varepsilon(\mathbf{m}) = A(\nabla\mathbf{m})^2 + \varepsilon_{\text{DMI}} + K_u m_z^2$$
$$- 0.5 M_s \mathbf{m} \cdot \mathbf{H}_m - M_s \mathbf{m} \cdot \mathbf{H}_{\text{ext}}. \quad (2)$$

$\varepsilon_{\text{DMI}} = D[m_z(\nabla \cdot \mathbf{m}) - (\mathbf{m} \cdot \nabla)m_z]$ is the interfacial DMI energy density, m_z is the magnetization *z* component, $\mathbf{H}_m$ is the magnetostatic field, and $\mathbf{H}_{\text{ext}}$ is the external magnetic field. The Néel skyrmion is a metastable state with respect to the uniform state (skyrmion energy is larger than the uniform one) for $4 \ \mu\text{T} \leqslant \mu_0 H_\perp < 150$ mT, while it becomes a stable state for $0 \leqslant \mu_0 H_\perp < 4 \ \mu\text{T}$ (see Fig. 5). These results qualitatively explain the collapsing dynamics in sample No. 1 [Fig. 2(a), and Figs. 4(a)–4(e)]. In particular, the pure Néel skyrmions are metastable for $\mu_0 H_\perp \leqslant 141$ mT, then become stable in the range of -92.3 mT $< \mu_0 H_\perp < 0$ mT, giving rise to a phase transition to labyrinth domains, and eventually become again metastable states for higher fields (the energetic stability is symmetric upon the field reversal).

The effect of external fields on the hybrid skyrmions in sample No. 2 can be understood from early results on magnetic bubbles in bulk materials [39–43]. In this scenario, we can identify three cases according to the value of the quality factor $Q = 2K_u/\mu_0 M_s^2$:

Sample #1, Pure Néel skyrmion

Sample #2, Hybrid skyrmion

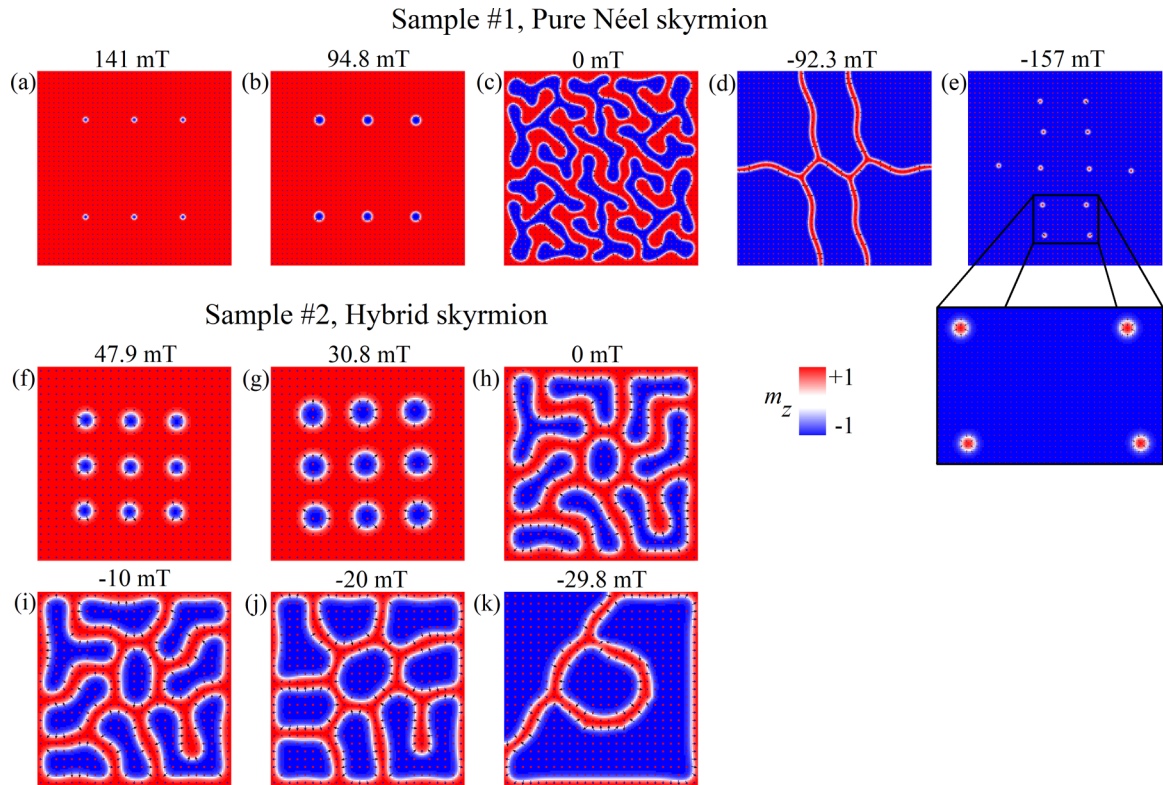

FIG. 4. Micromagnetic simulation results of the collapsing dynamics in the top layer of the two samples, No. 1 and No. 2.

(1) $Q < 1$, the perpendicular anisotropy, is weaker than the magnetostatic field; hence, the easy axis is in plane and vortices are the stable solution in infinite film [44]. However, if the sample dimensions are reduced below a threshold value and the sample thickness is increased, magnetic bubbles with a large domain wall can be still stabilized (the confinement effect is crucial).

(2) $1 < Q < 2$, the perpendicular anisotropy, is comparable or larger than the magnetostatic field. The easy axis is out of plane and magnetic bubbles are the energetically favored solution for large sample dimensions, even at zero external field [39].

(3) $Q > 2$, the perpendicular anisotropy, is much larger than the magnetostatic field. The easy axis is out of plane

and magnetic bubbles are observed at zero field, as a result of the confinement effect in sufficiently small samples [41], whereas, for the larger dots, random labyrinth domains are obtained at zero field.

In sample No. 2, the quality factor is 1 or slightly larger; therefore, the discussion of point 2 supports our results. We wish to underline that the energy landscape for stabilizing hybrid skyrmions and magnetic bubbles is very similar, i.e., they are both energetically favored solutions of the magnetostatic energy minimization. Therefore, the response of a magnetic bubble to external fields is expected to be qualitatively similar to that of a hybrid skyrmion in a low/zero IDMI multilayer. Indeed, Fig. 6 shows our simulations for a magnetic bubble of a bulk materials with a perpendicular magnetic anisotropy and
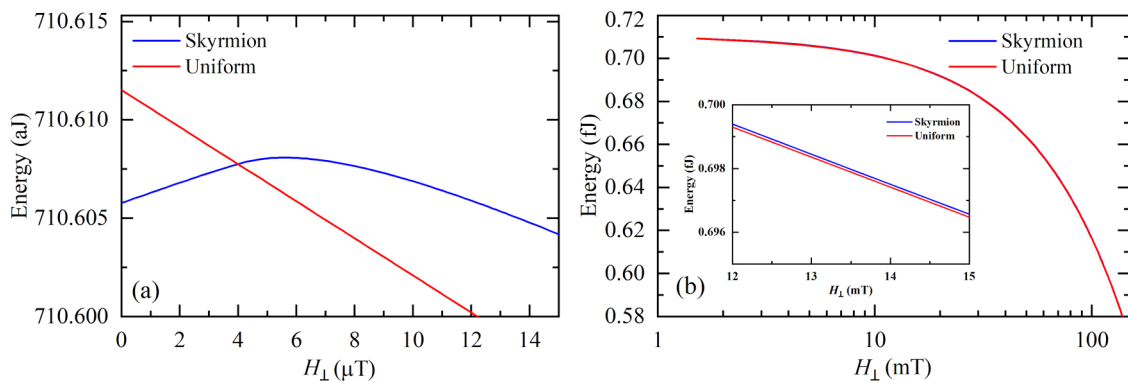

FIG. 5. Comparison between the skyrmion and uniform energies as a function of the perpendicular field, as computed from the minimization of the energy functional [38]. (a) Energies in the field range $0\ \mu T \leqslant \mu_0 H_\perp < 15\ \mu T$, where the transition field of 4 μT is evident. (b) Energies in the field range $0\ mT \leqslant \mu_0 H_\perp \leqslant 150\ mT$ in a logarithmic scale. Inset in (b): Magnified section of the energies in the field range $12\ mT \leqslant \mu_0 H_\perp \leqslant 15\ mT$ to show that the skyrmion is a metastable state.
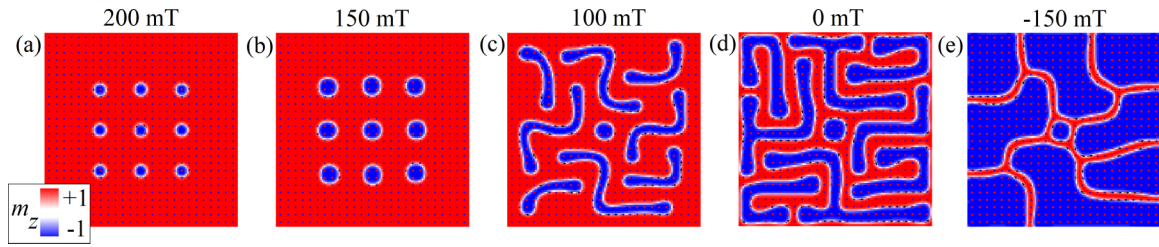
FIG. 6. Micromagnetic simulation results of the collapsing dynamics of magnetic bubbles in a perpendicular bulk material.

zero IDMI, which has the same parameters and geometrical dimensions as the previous multilayer sample No. 2. The number of magnetic bubbles (Bloch skyrmions) is also the same. We observe a qualitatively similar field response, where magnetic bubbles are initially stabilized by a positive field ($\mu_0 H_\perp = 200$ mT). As the field decreases, magnetic bubbles transform into wormlike shapes. After reversing the direction of field, large band domains appear with the core magnetization parallel to the negative field ($\mu_0 H_\perp = -150$ mT).

However, we wish to point out that two key differences exist between bulk samples and multilayers hosting hybrid skyrmions, which do not affect our conclusions: (i) in multilayers, each ferromagnetic layer is coupled only through dipolar interactions, and (ii) the IDMI can be only introduced in multilayers due to the presence of asymmetric interfaces where the ferromagnetic layers are thin (typically with a thickness smaller than 1 nm).

To get a deeper understanding of the collapsing dynamics of skyrmions in magnetic multilayers, we perform massive micromagnetic simulations as a function of the material parameters, which is summarized in Fig. 7, where a collapsing dynamics diagram in the Q–d ($d = 2A/D$) space is illustrated [38]. We identify five main regions:

(a) For $Q < 1$ and $0 \leqslant d \leqslant 0.55$ (blue region): The initial state contains hybrid skyrmions (HS) after relaxation and they undergo collapsing dynamics similar to the sample No. 1 (collapsing dynamics type 1, which lead to wormlike domains as the field is reduced to zero, and to a mixed phase as the field is reversed and equal to -100 mT (see Fig. 8). In particular, the mixed phase includes hybrid skyrmions and magnetic bubbles. This is because the IDMI is not sufficiently large to fix the skyrmion helicity throughout the layers.

(b) For $1 \leqslant Q \leqslant 1.25$ and $0 \leqslant d \leqslant 0.5$ (red region): The initial state contains hybrid skyrmions after relaxation. The dynamics type 2 are similar to the results of sample No. 2, meaning conversion of the hybrid skyrmions into large band domains as the field decreases and reverses its sign. Indeed, the experimental magnetic parameters of sample No. 2 fall in this region, as indicated by the black star.

(c) For $1.25 < Q \leqslant 1.4$ and $0.2 \leqslant d \leqslant 0.4$ (red region): The initial state contains pure Néel skyrmions (PNS) after relaxation. However, the collapsing dynamics are similar to sample No. 2 (collapsing dynamics type 2) and large band domains are obtained in the end.

(d) For $1.25 < Q \leqslant 1.4$ and $0 \leqslant d \leqslant 0.3$ (yellow region): The equilibrium configuration is the uniform out-of-plane state because the perpendicular magnetic anisotropy is too high to allow the existence of skyrmions.

(e) For $1 \leqslant Q \leqslant 1.4$ and $0.5 < d \leqslant 1$ (green region): The initial state contains pure Néel skyrmions after relaxation. The dynamics type 1 are similar to the results of sample No. 1, meaning that skyrmions undergo two phase transitions to labyrinth domains and Néel skyrmions with opposite polarity. Indeed, the experimental magnetic parameters of sample No. 1 fall in this region, as indicated by the black star.

Based on the full phase diagram, we can conclude that when $1 < Q < 1.25$ for any given choice of d, and for $0.6 \leqslant d \leqslant 1$ for any given choice of Q, it is possible to establish a direct relation between the type of skyrmions and the collapsing dynamics, which are exactly the cases of our experimental observations.
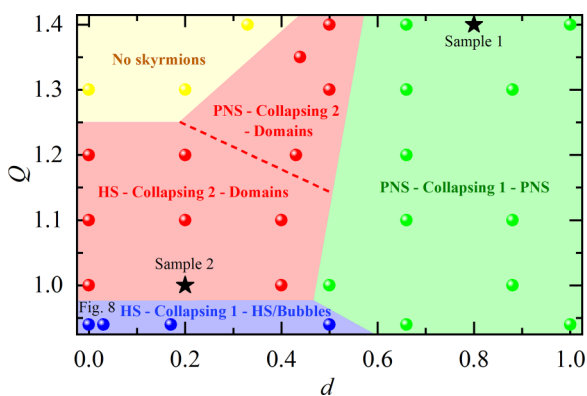

FIG. 7. Phase diagram that summarizes the collapsing dynamics in the Q–d space, which is obtained by micromagnetic simulations. Different colors are utilized to represent different states (pure Néel skyrmions: PNS, or hybrid skyrmions: HS) and the associated type of collapsing dynamics (type 1: similar to sample No.1, or type 2: similar to sample No. 2). Scattered symbols refer to the Q and d values used in the simulations. The black stars indicate the values of Q and d corresponding to the experimental samples No. 1 and No. 2, respectively. An example of collapsing dynamics concerning the blue region is illustrated in Fig. 8.

V. SUMMARY AND CONCLUSIONS

In summary, we have studied both experimentally and numerically the collapsing dynamics of magnetic skyrmions in two distinct experimental multilayers, where pure Néel and hybrid skyrmions exist. Both experimental observations and numerical results show two different collapsing behaviors which we ascribed to the competition between different
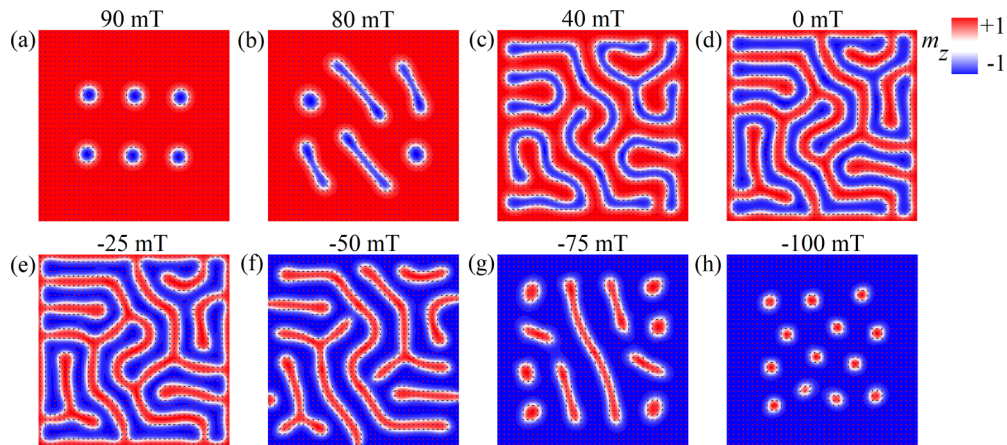
FIG. 8. Micromagnetic simulations of the collapsing dynamics type 1 of hybrid skyrmions to a mixed phase including hybrid skyrmions and bubbles for $Q = 0.94$ and $d = 0$.

energy terms. In IDMI-dominated system-[Pt/Co/Ir]$_{15}$ multilayer, such collapsing dynamics are consequences of the change of the energetic stability of pure Néel skyrmions due to the change of the external field. Skyrmions are metastable at $\mu_0 H_\perp = 141$ mT, then become stable or quasistable in the range 0 mT $< \mu_0 H_\perp < |92.3|$ mT, giving rise to a morphological transition to labyrinthine domains, and finally become metastable states with opposite cores for higher fields. On the contrary, in magnetostatic-dominated system-[Ta/CoFeB/MgO]$_{15}$ multilayer, hybrid skyrmions are characterized by reversible processes where the skyrmion cores expand following an increase of external fields, and merge together to form large band domains. Our work establishes an easily accessible technique to identify the type of skyrmion in a magnetic multilayer. Our results can be used as preliminary tests preceding the use of skyrmions in specific applications, since the skyrmion dynamics strongly depend on the static-equilibrium three-dimensional profile in magnetic multilayers.

[1] N. Nagaosa and Y. Tokura, Topological properties and dynamics of magnetic skyrmions, Nat. Nanotechnol. **8**, 899 (2013).

[2] A. Fert, V. Cros, and J. Sampaio, Skyrmions on the track, Nat. Nanotechnol. **8**, 152 (2013).

[3] G. Finocchio, F. Büttner, R. Tomasello, M. Carpentieri, and M. Kläui, Magnetic skyrmions: From fundamental to applications, J. Phys. D: Appl. Phys. **49**, 423001 (2016).

[4] T. Dohi, R. M. Reeve, and M. Kläui, Thin film skyrmionics, Annu. Rev. Condens. Matter Phys. **13**, 73 (2022).

[5] S. Mühlbauer, B. Binz, F. Jonietz, C. Pfleiderer, A. Rosch, A. Neubauer, R. Georgii, and P. Böni, Skyrmion lattice in a chiral magnet, Science **323**, 915 (2009).

[6] A. Neubauer, C. Pfleiderer, B. Binz, A. Rosch, R. Ritz, P. G. Niklowitz, and P. Böni, Topological Hall Effect in the A Phase of MnSi, Phys. Rev. Lett. **102**, 186602 (2009).

[7] X. Z. Yu, Y. Onose, N. Kanazawa, J. H. Park, J. H. Han, Y. Matsui, N. Nagaosa, and Y. Tokura, Real-space observation of a two-dimensional skyrmion crystal, Nature (London) **465**, 901 (2010).

[8] S. X. Huang and C. L. Chien, Extended Skyrmion Phase in Epitaxial FeGe(111) Thin Films, Phys. Rev. Lett. **108**, 267201 (2012).

[9] F. Zheng, F. N. Rybakov, A. B. Borisov, D. Song, S. Wang, Z.-A. Li, H. Du, N. S. Kiselev, J. Caron, A. Kovács, M. Tian, Y. Zhang, S. Blügel, and R. E. Dunin-Borkowski, Experimental observation of chiral magnetic bobbers in B20-type FeGe, Nat. Nanotechnol. **13**, 451 (2018).

[10] A. S. Ahmed, J. Rowland, B. D. Esser, S. R. Dunsiger, D. W. McComb, M. Randeria, and R. K. Kawakami, Chiral bobbers and skyrmions in epitaxial FeGe/Si(111) Films, Phys. Rev. Mater. **2**, 041401(R) (2018).

[11] A. Soumyanarayanan, N. Reyren, A. Fert, and C. Panagopoulos, Emergent phenomena induced by spin–orbit coupling at surfaces and interfaces, Nature (London) **539**, 509 (2016).

[12] Z. Wang, M. Guo, H.-A. Zhou, L. Zhao, T. Xu, R. Tomasello, H. Bai, Y. Dong, S.-G. Je, W. Chao, H.-S. Han, S. Lee, K.-S. Lee, Y. Yao, W. Han, C. Song, H. Wu, M. Carpentieri, G. Finocchio, M.-Y. Im, S.-Z. Lin, and W. Jiang, Thermal generation,

manipulation and thermoelectric detection of skyrmions, Nat. Electron. **3**, 672 (2020).

[13] W. Jiang, P. Upadhyaya, W. Zhang, G. Yu, M. B. Jungfleisch, F. Y. Fradin, J. E. Pearson, Y. Tserkovnyak, K. L. Wang, O. Heinonen, S. G. E. Te Velthuis, and A. Hoffmann, Blowing magnetic skyrmion bubbles, Science **349**, 283 (2015).

[14] O. Boulle, J. Vogel, H. Yang, S. Pizzini, D. de Souza Chaves, A. Locatelli, T. O. Menteş, A. Sala, L. D. Buda-Prejbeanu, O. Klein, M. Belmeguenai, Y. Roussigné, A. Stashkevich, S. M. Chérif, L. Aballe, M. Foerster, M. Chshiev, S. Auffret, I. M. Miron, and G. Gaudin, Room-temperature chiral magnetic skyrmions in ultrathin magnetic nanostructures, Nat. Nanotechnol. **11**, 449 (2016).

[15] W. Jiang, X. Zhang, G. Yu, W. Zhang, X. Wang, M. Benjamin Jungfleisch, J. E. Pearson, X. Cheng, O. Heinonen, K. L. Wang, Y. Zhou, A. Hoffmann, and S. G. E. te Velthuis, Direct observation of the skyrmion Hall effect, Nat. Phys. **13**, 162 (2017).

[16] C. Moreau-Luchaire, C. Moutafis, N. Reyren, J. Sampaio, C. A. F. Vaz, N. Van Horne, K. Bouzehouane, K. Garcia, C. Deranlot, P. Warnicke, P. Wohlhüter, J. M. George, M. Weigand, J. Raabe, V. Cros, and A. Fert, Additive interfacial chiral interaction in multilayers for stabilization of small individual skyrmions at room temperature, Nat. Nanotechnol. **11**, 444 (2016).

[17] S. Woo, K. Litzius, B. Krüger, M. Y. Im, L. Caretta, K. Richter, M. Mann, A. Krone, R. M. Reeve, M. Weigand, P. Agrawal, I. Lemesh, M. A. Mawass, P. Fischer, M. Kläui, and G. S. D. Beach, Observation of room-temperature magnetic skyrmions and their current-driven dynamics in ultrathin metallic ferromagnets, Nat. Mater. **15**, 501 (2016).

[18] K. Litzius, I. Lemesh, B. Krüger, P. Bassirian, L. Caretta, K. Richter, F. Büttner, K. Sato, O. A. Tretiakov, J. Förster, R. M. Reeve, M. Weigand, I. Bykova, H. Stoll, G. Schütz, G. S. D. Beach, and M. Kläui, Skyrmion Hall effect revealed by direct time-resolved x-ray microscopy, Nat. Phys. **13**, 170 (2017).

[19] A. Soumyanarayanan, M. Raju, A. L. G. Oyarce, A. K. C. Tan, M. Y. Im, A. P. Petrovic, P. Ho, K. H. Khoo, M. Tran, C. K. Gan, F. Ernult, and C. Panagopoulos, Tunable room-temperature magnetic skyrmions in Ir/Fe/Co/Pt multilayers, Nat. Mater. **16**, 898 (2017).

[20] F. Büttner, I. Lemesh, M. Schneider, B. Pfau, C. M. Günther, P. Hessing, J. Geilhufe, L. Caretta, D. Engel, B. Krüger, J. Viefhaus, S. Eisebitt, and G. S. D. Beach, Field-free deterministic ultrafast creation of magnetic skyrmions by spin–orbit torques, Nat. Nanotechnol. **12**, 1040 (2017).

[21] K. Zeissler, S. Finizio, K. Shahbazi, J. Massey, F. Al Ma'Mari, D. M. Bracher, A. Kleibert, M. C. Rosamond, E. H. Linfield, T. A. Moore, J. Raabe, G. Burnell, and C. H. Marrows, Discrete Hall resistivity contribution from Néel skyrmions in multilayer nanodiscs, Nat. Nanotechnol. **13**, 1161 (2018).

[22] D. Maccariello, W. Legrand, N. Reyren, K. Garcia, K. Bouzehouane, S. Collin, V. Cros, and A. Fert, Electrical detection of single magnetic skyrmions in metallic multilayers at room temperature, Nat. Nanotechnol. **13**, 233 (2018).

[23] W. Li, I. Bykova, S. Zhang, G. Yu, R. Tomasello, M. Carpentieri, Y. Liu, Y. Guang, J. Gräfe, M. Weigand, D. M. Burn, G. der Laan, T. Hesjedal, Z. Yan, J. Feng, C. Wan, J. Wei, X. Wang, X. Zhang, H. Xu, C. Guo, H. Wei, G. Finocchio, X. Han, and G. Schütz, Anatomy of skyrmionic textures in magnetic multilayers, Adv. Mater. **31**, 1807683 (2019).

[24] Y. Guang, L. Zhang, J. Zhang, Y. Wang, Y. Zhao, R. Tomasello, S. Zhang, B. He, J. Li, Y. Liu, J. Feng, H. Wei, M. Carpentieri, Z. Hou, J. Liu, Y. Peng, Z. Zeng, G. Finocchio, X. Zhang, J. M. D. Coey, X. Han, and G. Yu, Electrical detection of magnetic skyrmions in a magnetic tunnel junction, Adv. Electron. Mater. **9**, 2200570 (2023).

[25] S. Woo, K. M. Song, X. Zhang, Y. Zhou, M. Ezawa, X. Liu, S. Finizio, J. Raabe, N. J. Lee, S.-I. Kim, S.-Y. Park, Y. Kim, J.-Y. Kim, D. Lee, O. Lee, J. W. Choi, B.-C. Min, H. C. Koo, and J. Chang, Current-driven dynamics and inhibition of the skyrmion Hall effect of ferrimagnetic skyrmions in GdFeCo films, Nat. Commun. **9**, 959 (2018).

[26] L. Caretta, M. Mann, F. Büttner, K. Ueda, B. Pfau, C. M. Günther, P. Hessing, A. Churikova, C. Klose, M. Schneider, D. Engel, C. Marcus, D. Bono, K. Bagschik, S. Eisebitt, and G. S. D. Beach, Fast current-driven domain walls and small skyrmions in a compensated ferrimagnet, Nat. Nanotechnol. **13**, 1154 (2018).

[27] T. Dohi, S. DuttaGupta, S. Fukami, and H. Ohno, Formation and current-induced motion of synthetic antiferromagnetic skyrmion bubbles, Nat. Commun. **10**, 5153 (2019).

[28] W. Legrand, D. Maccariello, F. Ajejas, S. Collin, A. Vecchiola, K. Bouzehouane, N. Reyren, V. Cros, and A. Fert, Room-temperature stabilization of antiferromagnetic skyrmions in synthetic antiferromagnets, Nat. Mater. **19**, 34 (2020).

[29] R. Juge, N. Sisodia, J. U. Larrañaga, Q. Zhang, V. T. Pham, K. G. Rana, B. Sarpi, N. Mille, S. Stanescu, R. Belkhou, M.-A. Mawass, N. Novakovic-Marinkovic, F. Kronast, M. Weigand, J. Gräfe, S. Wintz, S. Finizio, J. Raabe, L. Aballe, M. Foerster, M. Belmeguenai, L. D. Buda-Prejbeanu, J. Pelloux-Prayer, J. M. Shaw, H. T. Nembach, L. Ranno, G. Gaudin, and O. Boulle, Skyrmions in synthetic antiferromagnets and their nucleation via electrical current and ultra-fast laser illumination, Nat. Commun. **13**, 4807 (2022).

[30] A.-O. Mandru, O. Yıldırım, R. Tomasello, P. Heistracher, M. Penedo, A. Giordano, D. Suess, G. Finocchio, and H. J. Hug, Coexistence of distinct skyrmion phases observed in hybrid ferromagnetic/ferrimagnetic multilayers, Nat. Commun. **11**, 6365 (2020).

[31] O. Yıldırım, R. Tomasello, Y. Feng, G. Carlotti, S. Tacchi, P. M. Vaghefi, A. Giordano, T. Dutta, G. Finocchio, H. J. Hug, and A.-O. Mandru, Tuning the coexistence regime of incomplete and tubular skyrmions in ferromagnetic/ferrimagnetic/ferromagnetic trilayers, ACS Appl. Mater. Interfaces **14**, 34002 (2022).

[32] W. Legrand, J.-Y. Chauleau, D. Maccariello, N. Reyren, S. Collin, K. Bouzehouane, N. Jaouen, V. Cros, and A. Fert, Hybrid chiral domain walls and skyrmions in magnetic multilayers, Sci. Adv. **4**, eaat0415 (2018).

[33] N. K. Duong, R. Tomasello, M. Raju, A. P. Petrović, S. Chiappini, G. Finocchio, and C. Panagopoulos, Magnetization reversal signatures of hybrid and pure Néel skyrmions in thin film multilayers, APL Mater. **8**, 111112 (2020).

[34] I. Lemesh and G. S. D. Beach, Twisted domain walls and skyrmions in perpendicularly magnetized multilayers, Phys. Rev. B **98**, 104402 (2018).

[35] A. Giordano, G. Finocchio, L. Torres, M. Carpentieri, and B. Azzerboni, Semi-implicit integration scheme for Landau-Lifshitz-Gilbert-Slonczewski equation, J. Appl. Phys. **111**, 2010 (2012).

[36] S. Rohart and A. Thiaville, Skyrmion confinement in ultrathin film nanostructures in the presence of Dzyaloshinskii-Moriya interaction, Phys. Rev. B **88**, 184422 (2013).

[37] R. Tomasello, M. Carpentieri, and G. Finocchio, Influence of the Dzyaloshinskii-Moriya interaction on the spin-torque diode effect, J. Appl. Phys. **115**, 17C730 (2014).

[38] R. Tomasello, K. Y. Guslienko, M. Ricci, A. Giordano, J. Barker, M. Carpentieri, O. Chubykalo-Fesenko, and G. Finocchio, Origin of temperature and field dependence of magnetic skyrmion size in ultrathin nanodots, Phys. Rev. B **97**, 060402(R) (2018).

[39] S. Komineas, C. A. F. Vaz, J. A. C. Bland, and N. Papanicolaou, Bubble domains in disc-shaped ferromagnetic particles, Phys. Rev. B **71**, 060405(R) (2005).

[40] T. Liu, V. Puliafito, F. Montaigne, S. Petit, C. Deranlot, S. Andrieu, O. Ozatay, G. Finocchio, and T. Hauet, Reproducible formation of single magnetic bubbles in an array of patterned dots, J. Phys. D: Appl. Phys. **49**, 245002 (2016).

[41] C. Moutafis, S. Komineas, C. A. F. Vaz, J. A. C. Bland, T. Shima, T. Seki, and K. Takanashi, Magnetic bubbles in FePt nanodots with perpendicular anisotropy, Phys. Rev. B **76**, 104426 (2007).

[42] J. Choi, J. Wu, C. Won, Y. Z. Wu, A. Scholl, A. Doran, T. Owens, and Z. Q. Qiu, Magnetic Bubble Domain Phase at the Spin Reorientation Transition of Ultrathin Fe/Ni/Cu(001) Film, Phys. Rev. Lett. **98**, 207205 (2007).

[43] G. D. Skidmore, A. Kunz, C. E. Campbell, and E. D. Dahlberg, Micromagnetic domain structures in cylindrical nickel dots, Phys. Rev. B **70**, 012410 (2004).

[44] C. Moutafis, S. Komineas, C. A. F. Vaz, J. A. C. Bland, and P. Eames, Vortices in ferromagnetic elements with perpendicular anisotropy, Phys. Rev. B **74**, 214406 (2006).

[45] www.petaspin.com